# Improved limit of detection of a high-resolution fs-LIMS instrument through mass-selective beam blanking

Salome Gruchola[*], Coenraad P. de Koning, Reto Wiesendanger, Peter Keresztes Schmidt, Andreas Riedo, Valentine Grimaudo, Rustam A. Lukmanov, Niels F.W. Ligterink, Marek Tulej, Peter Wurz

*Physics Institute, Space Research and Planetary Sciences, University of Bern, Sidlerstrasse 5, CH-3012, Bern, Switzerland*

A B S T R A C T

Laser Ablation Ionisation Mass Spectrometry (LIMS) is an important quantitative method for chemical analysis of solids. Current limits of detections (LoDs) of LIMS instruments are in the ppm to sub-ppm range (atomic fractions), while other commonly used techniques for solid sample analysis reach LoDs at ppb levels or even below. This study presents the implementation of mass-selective beam blanking in the Laser Mass Spectrometer − Gran Turismo (LMS-GT) to improve the instruments' detection limit. LMS-GT is a high-performance time-of-flight LIMS instrument coupled to a femtosecond laser ablation ion source reaching micrometre spatial resolutions and mass resolutions $\gtrsim$ 12′000. A fast high voltage switch was developed in-house to induce potential changes at an Einzel lens at the intermediate time focus of the ion trajectory, leading to short deflections of the ion beam and hindering selected species from reaching the detector. The intensities of single mass lines are reduced with 100% efficiency to below the noise floor when blanked. The detector gain can safely be increased while blanking the most intense mass lines simultaneously, thus improving the detection limit. The LoD of LMS-GT prior to the installation of the mass-selective blanking device was at ppm level (at. frac.) with few sub-ppm detections, the installation pushed it to the lower ppb range, without compromising the initial performance. This emphasises that fs-LIMS can be a powerful quantitative technique for the chemical analysis of solids, with the potential to reach the levels of mass spectrometric analysis achievable with Secondary Ion Mass Spectrometry (SIMS) and Laser Ablation−Inductively Coupled Plasma−Mass Spectrometry (LA-ICP-MS).

© 2022 Published by Elsevier B.V.

## 1. Introduction

The technique of mass spectrometry has undergone a remarkable evolution in the last few decades, bringing forth various instruments applicable to a wide range of fields of research and development in academia and industry, among which are material sciences [1], mineralogy [2], planetary and space sciences [3−5], cosmochemistry and astrobiology [6,7], and the semiconductor industry [8]. The field of interest narrows down the potential instrument types and sets the requirements for the instrument parameters, with some of the most important ones being mass resolution, lateral and vertical resolution, sensitivity, limit of detection (LoD), dynamic range, acquisition speed, weight, and

power consumption. No instrument can excel in all disciplines but pushing the limits to extend the parametric range has always been an important discipline in research. This work contributes to the field by applying the technique of mass-selective beam blanking to a laser ablation ionisation mass spectrometer (LIMS) with the aim of improving its LoD.

The LoD is defined as the lowest concentration that the system can distinguish from the background. It should not be mistaken for the term sensitivity, which is defined as the slope of the calibration curve which is equivalent to the ratio between the analyte signal intensity and the analyte concentration [9]. Therefore, sensitivity does not take the noise level into account, and it is possible for an instrument to be very sensitive while simultaneously suffering from significant noise which leads to a very modest LoD. There is a further distinction between mass sensitivity and concentration sensitivity and the terms should be handled carefully [10]. Mass and concentration sensitivity describe the capability of the

instrument to measure elements with certain weight and particle fractions in the sample, respectively. The two are not equivalent since different elements differ in mass. The sensitivity is usually also not linear over the concentration range and is rather described by a non-linear function of the analyte concentration. The concentration at which this curve intersects the signal level (nominally at three times the signal baseline) is then defined as the LoD. Contrary to the sensitivity, the LoD is a fixed value for a given species under constant conditions.

The instruments with the lowest LoDs available nowadays can be found amongst laser induced plasma mass spectrometry (LA-ICP-MS), glow discharge mass spectrometry (GDMS) and secondary ion mass spectrometry (SIMS) [11]. LA-ICP-MS has detection limits at the sub-ppb g/g level, enabling detections of ultra-trace elements. The detections are, however, complicated by matrix effects and matrix-matched calibration standards are required for quantitative analysis [12,13]. Similarly, GDMS reaches detection limits below the ppb g/g level for both conductive and non-conductive samples. For single components without interference, low resolution, and long acquisition time, the LoD can even drop below the ppt g/g level (weight fractions) [14,15]. Especially for conductive samples the sample handling is simple, and the method is suitable for depth profiling [16]. SIMS offers LoDs in the lower ppb (atomic fractions) range (TOF-SIMS) and even lower ppt (at. frac.) range (dynamic SIMS). The technique is mostly used for surface analysis because of its limited sampling depth compared to laser-based techniques or GDMS [17]. The price to pay for such ultra-high detection limits is the reduced spatial resolution. The detection limit of an instrument is, to a certain point, constrained by the analytical spot size. The spatial resolution together with the sampling depth determine the amount of analysed material which then determines the physical LoD. When the LoD is reached, improving the spatial resolution will require the sample to be probed deeper, resulting in the same amount of material analysed and therefore not improving the LoD of the instrument. Instruments which are limited in depth analysis reach better limits of detection for bigger analytical spot sizes. Dynamic SIMS reaches LoD of 10 ppt (atomic range) only for analytical spot sizes of around $20-100$ μm, for smaller spot sizes of 1 μm, the LoD is a factor 1000 higher at 10 ppb (at. frac.) [11].

The instrument used for this study is LMS-GT, a laboratory-scale laser ablation ionisation mass spectrometer (LIMS) coupled with a time-of-flight (TOF) mass analyser. The LIMS method uses pulsed lasers for the ablation, atomisation, and ionisation of the sample material and mass analysers (typically TOF mass spectrometers) for the measurement of the atomic ions (typically positively charged species) to determine the elemental (isotopic) composition of the studied material [18,19]. LIMS equipped with a femtosecond ablation ion source (fs-LIMS) has become a reliable method for chemical analysis, high-precision depth profiling and surface imaging, which allow to infer surface heterogeneity at micron or submicron scales [20]. The fs-LIMS technique is applicable to practically any solid sample, simultaneously measuring all elements (apart from noble gases) over the full mass range simultaneously, including elements with high ionisation potentials. Improvements to the ionisation efficiency of atoms and a reduction of cluster production can be achieved with a double pulse ion source (DP) [21–23]. The LIMS technique is not yet as sensitive as LA-ICP-MS with a LoD at ppm levels (at. frac.), in specific cases down to ppb levels. However, only little to no sample preparation is required, which makes LIMS, in contrast to the operationally complex LA-ICP-MS and SIMS instruments, a powerful tool for *in-situ* applications. The LoD of the instrument before the installation of the mass-selective blanking device was at the ppm level (at. frac.) [24]. For equal spot sizes, the LoD of LMS-GT is comparable to state-of-the-art TOF-SIMS

instruments. TOF-SIMS can, however, reach spatial resolutions down to 100 nm, nano-SIMS even down to 50 nm [11,25]. LIMS instruments were reported to reach equally good spatial resolutions down to 50 nm by using a tip-enhanced ablation technique [26].

The goal of the work presented here was to improve the LoD of the LMS-GT instrument using mass-selective beam blanking, with which selected mass lines can be removed from recorded TOF spectra by hindering the corresponding ions from reaching the detector. If the most intense peaks are removed from a spectrum, the detector voltage can be safely increased by a certain amount dictated by the intensities of the remaining peaks without damaging the preamplifier of the acquisition card or leading to non-linear saturation effects of the detector. By increasing the detector voltage, its gain is increased as well, resulting in higher signal-to-noise ratios (SNR) of the remaining peaks and thus, mass lines previously hidden in the noise floor can be made detectable. This improves the dynamic range on the electronics side and therefore the instruments' LoD. A high number of ions impacting on the detector at the same time can lead to temporary gain loss through charge depletion and the detector will need to recharge for a certain amount of time, making it less sensitive to the ions impacting in the meantime. Their abundances will therefore be underestimated. For low intensity peaks not exceeding the linearity limit of the detector, recharge times are in the order of nanoseconds. Since ion packages in TOF spectra recorded with the current voltage settings of LMS-GT are typically separated by (several) hundreds of nanoseconds, such recharge times do not impact the sensitivity of the following ions. Accurately quantifying the detector recharge time after intense ion signals is, however, complicated because of its dependence on many highly non-linear effects such as ion rate per time and ion rate per area. A possible solution is to remain in the linear region, e.g., by lowering the detector voltage such that the peaks remain of relatively low intensity. This, however, will not allow for measuring low abundant elements. Instead, one can blank the high intensity mass peaks which would lead to the occurrence of non-linear saturation effects and gain loss, thus remaining in the linear region without having to decrease the detector voltage.

A further advantage that comes with blanking single high intensity mass lines is a reduction of distortions of the baseline following intense peaks (due to, e.g., electronic ringing caused by the front-end electronics), which influence subsequent mass lines. Especially when doing quantitative calculations as for example isotope studies, accurate determination of the peak areas is of high importance and having a minimally distorted baseline will allow for a more accurate signal integration and hence yield more reliable results. The SNRs of small peaks can also be increased to some extent by using increased laser irradiances. However, this does not prevent baseline distortions or the gain loss of the detector typically occurring after an intense mass peak. In principle, when blanking certain mass lines, the relative abundance of species in the ion population reaching the detector differs from the relative abundance in the sample, which might need to be considered during data analysis.

To hinder certain species from reaching the detector, the ion beam needs to be deflected for a short amount of time, precisely timed to only affect the selected ion package(s), while letting the adjacent ones reach the detector without transmission losses. The deflection can be realised with a short voltage pulse applied to one or more electrodes along the beam path. The potentials of the ion optical elements are carefully adjusted and optimised to minimise transmission losses and maximise the resolution. Changing the potentials on certain electrodes can therefore have a large impact on the transmission of the affected ion packages. To only affect

single ion packages, the voltage switch needs to be fast and operated at a time focus, otherwise it is not possible to influence just one single ion package.

This method of mass-selective blanking was successfully introduced to the RTOF instrument, a reflectron time-of-flight mass spectrometer, which was part of the Rosina instrument on-board the Rosetta mission [27]. A Hardmirror consisting of an Einzel lens followed by a very short ion mirror and a backplane was selected for beam blanking. The Hardmirror had the general task of reflecting the ion beam to double the flight path. To additionally use it for mass-selective blanking, a short electrical pulse was applied to the potential of the Hardmirror's backplane electrode when the species that was selected for blanking was just passing through the Hardmirror. This defocused the ion package such that it no longer reached the detector. The intensity of the selected mass line was reduced by a factor of more than 1000. Even though the Hardmirror was located at a time focus, the temporal focusing of the ion packages was not sufficient to allow blanking single mass lines while leaving neighbouring mass lines unaffected by the pulse. The higher the suppression of the selected mass line, the higher was the impact on the intensities of adjacent mass lines [27].

Mass blanking has also previously been applied in MALDI-TOF [28] and laser desorption TOF [29] instruments, where it is more commonly known under (timed) mass gating or timed ion selection (TIS). Timed mass gating, which uses rapidly switchable gates to allow ions of interest to pass, is more often used to extract a certain mass of interest from a spectrum, rather than blanking a single mass to record the remaining spectrum [28] and is therefore not suitable for the desired application. The method of blanking a certain mass range by a HV pulse was also implemented in the LMS instrument [30], a miniature LIMS-TOF instrument, specifically designed for *in-situ* space explorations, which is in many ways LMS-GT's predecessor [31]. However, due to the limited size of the TOF mass analyser, removal of single mass lines was not achieved with this setup [30]. Another instrument that uses blanking for mass selection is the laser desorption tandem-TOF mass spectrometer by Ref. [32], where a short HV pulse is applied to a split Einzel lens located approximately in the middle of the ion trajectory to deflect the ion beam [33]. The tandem-TOF instrument has a z-shaped ion trajectory with two ion mirrors and therefore shares several similarities with the LMS-GT instrument operated in this work [32,34]. Although blanking of single mass lines is not possible with this tandem-TOF instrument, the method of beam deflection was deemed optimally suitable for LMS-GT, mainly due to the similarities between the instruments, the ease of the implementation, and the progress of fast electronics in the last three decades. Additionally, blanking of single mass lines was previously achieved through a pulsed-pin ion gate [35,36], installed in another laser desorption tandem-TOF instrument (LD-TOF-MS/MS). However, this method would require substantial changes to the LMS-GT instrument and was therefore deemed unsuitable. Beam blanking location, requirements for the electronics and the instrument modifications needed to achieve blanking of single mass lines all depend strongly on the geometry of the instrument and are described in the following.

## 2. Beam blanking in the LMS-GT instrument

### 2.1. The LMS-GT instrument

LMS-GT is a laser ablation and ionisation mass spectrometer located at the University of Bern, Switzerland. It is based on a similar ablation and detection principle as the much smaller LMS instrument, which was originally developed for *in-situ* analysis of Mercury's surface during the BepiColombo mission [13,31,37]. LMS-GT, using a TOF mass analyser with a doubly folded ion flight path of over 4 m, offers mass resolutions $(m/\Delta m) \gtrsim 12'000$ over a large mass range, which addresses the issue of isobaric interferences between polyatomic, monoatomic, and multiply charged species. LMS-GT uses a Ti:sapphire laser system (CPA-Series, Clark-MXR Inc., USA, $\lambda = 775$ nm, ~ 190 fs, 1 kHz) for laser ablation and ionisation. It produces a pulsed laser beam with maximum pulse energies of 1 mJ and high pulse-to-pulse energy stability (~ 4−8‰). Extensive studies on the design of LMS-GT and its quantitative performance were previously published [24,38]. The geometry will briefly be reviewed here.

A schematic view of the LMS-GT ion optics design is shown in Fig. 1. Ions produced from the sample by laser ablation and ionisation are accelerated by the ion source (SRC), which consists of a series of HV electrodes. After the ions leave the ion source, they are geometrically re-focused by two Einzel lenses (L1 and L2). A drift tube (DR1) connects the lenses to the first ion mirror (R1), which reduces the time spread of the ion packages and folds the ion trajectory. The first ion mirror is followed by two drift tubes (DR2 and DR3) with a third Einzel lens (L3) in-between. A second ion mirror (R2) reflects the beam a second time, which, after passing through another drift tube (DR4), hits the detector (DET1). The full ion flight path measures over 4 m, with L3 being located approximately in the middle. In total, the ions pass three time foci (TF1 to TF3) [38].

### 2.2. Mass-selective beam blanking

The three time foci are potential candidates for the installation of the mass-selective blanking device. At a time focus, the temporal spread, and thus the spatial spread, of the ion packages is minimised. The temporal separation of the ion packages at the blanking location determines how fast the voltage switch will have to operate; the smaller the separation between the ion packages the faster the voltage switch needs to be to allow for mass-selective ion blanking of a single mass line without interfering with neighbouring masses. Looking at the geometry shown in Fig. 1, one can see that the first (TF1) and the last (TF3) time focus cannot be considered for beam blanking, as the first one is located on the sample surface and the last one at the detector position. Only the second time focus (TF2), located in the middle of the ion trajectory at L3, can be considered and offers enough space for the installation of a beam blanking device.

The general purpose of L3 is to focus the ion beam. This should not be replaced for the ability to blank the beam, therefore, L3 was modified to support both. Being an electrostatic Einzel lens, L3 consists of three cylindrical ring electrodes with the two outer ones held on drift potential and the inner one on a floating potential. This is visualised in Fig. 2a. The outer ring electrodes are identical with a length of 38 mm, whereas the central ring electrode is much shorter with a length of only 5 mm. Simulations with the commercial ion optical software SIMION® (Scientific Instrument Services Inc.: SIMION ver. 8.0, Ringoes, NJ, USA) have shown that deflecting the ion beam by simply changing the voltage on one of the ring electrodes would require several kV. This would be a major complication for the blanking device electronics. A voltage pulse always introduces interferences and oscillations, and the higher the pulse amplitude and the faster the rise and fall times, the harder it is to constrain the oscillations. L3 is surrounded by sensitive electrodes which can easily be influenced by a large voltage pulse. Especially disturbances on the drift and ground potentials could become problematic as numerous electrodes including the detector are connected to drift and ground. This could disturb the ion times-of-flight and complicate the identification of species in a TOF spectrum or its calibration. A smaller pulse amplitude is therefore preferred, which cannot be realised by applying a different voltage on any of the electrodes of L3.
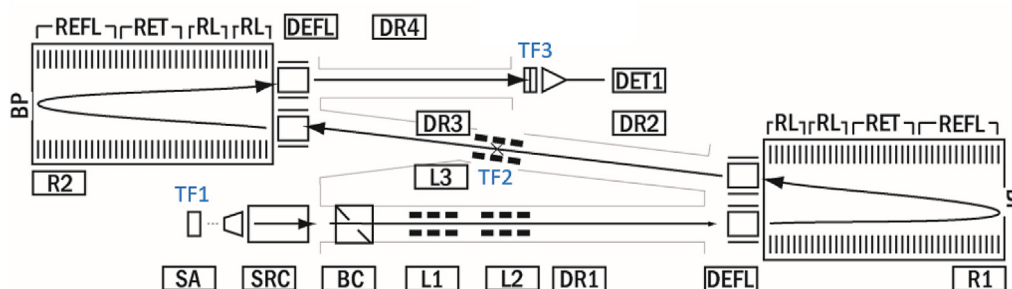
**Fig. 1.** Schematic view of the LMS-GT ion-optic design. Adapted with permission from Ref. [38]. Ions are ablated from the sample (SA) by laser radiation, then they are accelerated and focused onto the beam path by several ion optical elements. The ion optical elements include the ion source (SRC), three Einzel lenses (L1 to L3) and two ion mirrors (R1 and R2). Several drift tubes (DR1 to DR4) connect the ion optical elements along the beam path. The signal is recorded with a detector (DET1) at the end of the beam path. The locations of the three time foci (TF) are indicated.
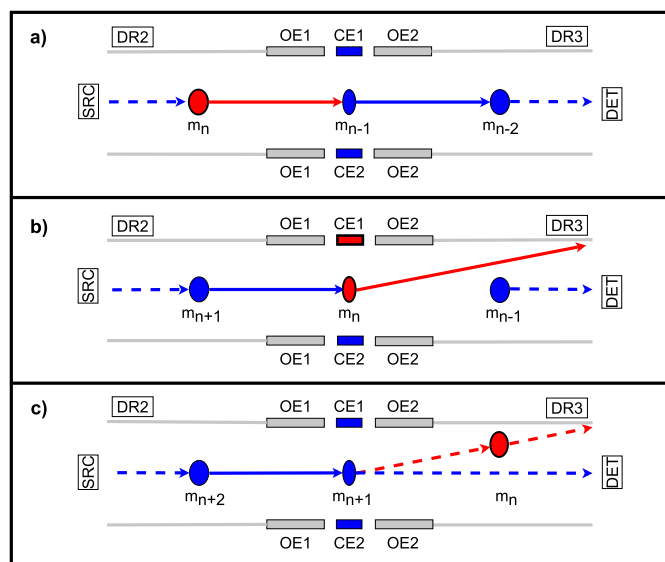


**Fig. 2.** Principle of beam blanking with an Einzel lens. The lens consists of two outer electrode rings (OE1 and OE2) and an inner electrode, split in two parts (CE1 and CE2). The outer electrodes OE1 and OE2 are held on drift potential ($-100$ V), as are the drift tubes (DR2 and DR3). Both CE1 and CE2 can be set to individual potentials. The ions are flying from left to right, i.e., from the source (SRC) to the detector (DET). The centre electrodes of the lens are situated at a time focus, the ion packages are therefore compressed inside the lens. For simplicity it is assumed that all ions are singly charged and the mass over charge ratio equals the mass. The goal is to blank the ion package with mass $m_n$. a) The ion package $m_n$ has not yet entered the lens, therefore, no blanking required and CE1 and CE2 are both set to the same floating potential. b) The ion package $m_n$ has now entered the Einzel lens and the voltage on CE1 is switched using the HV pulser, such that the ion package $m_n$ gets deflected onto a different trajectory. The electrode CE2 remains on float potential. The adjacent ion packages should be left unaffected by the voltage pulse. c) When the ion package $m_n$ has left the Einzel lens on its modified trajectory, the potential on CE1 can be switched back to the same potential as on CE2 to not influence the following ion package $m_{n+1}$. If this is successful, $m_{n+1}$ will continue again on the nominal trajectory and reach the detector, whereas the blanked ion package $m_n$ will eventually splat on the drift tube. This will leave it unrecorded by the acquisition system.

Instead, the central electrode of L3 was cut in half, dividing it into two half cylindrical electrodes with a slit of 2 mm in-between. The new geometry allows to set the potentials on each half individually. When no blanking is required, both halves can be held on the same float potential, acting as one ring electrode and yielding the same results as with the original lens. Adding a pulse to one half of the central electrodes will result in a potential difference normal to the ion trajectory. For a large enough potential difference, the ion beam will be deflected in such a way that it no longer reaches the detector. To blank single mass lines, a short voltage pulse is

required. The outer electrodes were considered as well for blanking, as they are longer and therefore a lower pulse amplitude would be sufficient to reach the same blanking efficiency as with the central electrodes. However, being longer electrodes has the disadvantage of not supporting single mass line blanking over the full mass range as the spatial separation between the ion packages decreases with increasing mass, which would lead to several ion packages being affected by one voltage pulse. This drawback is not present for the central electrode, at the prize of a slightly higher pulse amplitude. Simulations with the ion optical software SIMION using an ion population representing the NIST standard reference material (SRM) 664 showed that a pulse amplitude of $-400$ V should be sufficient to blank mass lines over the full mass range with 100% efficiency. The requirements of the voltage pulse were determined based on the predicted mass resolution of m/$\Delta$m $= 1000 - 2000$ at L3, resulting in a separation between ion packages of $\gtrsim 100$ ns. The concept of blanking single ion packages with the Einzel lens L3 is visualised in Fig. 2.

The option of applying two pulses of opposite polarity to the two parts of the central electrode was considered as well, as this would require smaller pulse amplitudes, e.g., $+200$ V and $-200$ V, potentially introducing less electronic noise to the system. However, the two pulses would need to be synchronised, which can be technically challenging for short pulse widths below 100 ns. Furthermore, applying two pulses instead of one is electronically more complicated and would require electronic hardware to support the two lens parts. One drawback of the modification of L3 is that it does have a relatively complicated form and it was not known prior to the installation of the new lens how heavily the adjacent masses would be affected by a blanking pulse. Simpler options like Bradbury-Nielsen gates exist, which have the advantage that the distance over which the deflecting field is felt is much shorter. However, they cannot achieve 100% blanking of a single mass line [39]. The biggest drawback of these gates is that they consist of a grid which is placed into the ion beam trajectory and therefore reduces the transmission of the instrument. Typical transmission values are around 1% [40]. Grid-type elements were not considered for mass-selective blanking in the LMS-GT instrument as it was built completely grid-less and optimised to support 100% transmission. Moreover, sputtering of ions from the grid might introduce spurious peaks in the mass spectra, which is of concern when analysing samples at the ppm to ppb level.

In Fig. 2 a simplified version of the Einzel lens L3 is shown, consisting of two outer electrodes (OE1 and OE2) and a centre electrode which was cut in half and now consists of two parts (CE1 and CE2). OE1 and OE2 are held on drift potential ($-100$ V) as are the two drift tubes (DR1 and DR2) which precede and follow L3, respectively. When no blanking is required, both CE1 and CE2 are

held on float potential. The ions enter the lens from the left and leave it on the right side, following the trajectory from the ion source (SRC) to the detector (DET). Fig. 2 visualises the process of blanking a mass line corresponding to mass $m_n$ in three timesteps. At a first time step, shown in Fig. 2a, mass $m_n$ has not yet entered the L3 and therefore, no blanking is required yet. Both CE1 and CE2 are held on float potential. In a next time step, shown in Fig. 2b, the ion package $m_n$ has entered the lens and the potential on CE1 is switched by using the HV pulser. This deflects $m_n$ onto a different trajectory. The adjacent ion packages $m_{n-1}$ and $m_{n+1}$ should not be affected by the pulse. In Fig. 2c the ion package $m_n$ has left L3 and the potential on CE1 can be switched back to float potential. $m_n$ will eventually splash on the drift tube and not reach the detector. It will therefore not be recorded by the acquisition system. The adjacent ion packages will continue on their nominal trajectory until they reach the detector.

The L3 lens needs to be supplied with different voltages. The outer electrodes (OE1 & OE2) are held on drift potential, which is provided by a single coaxial cable as the outer electrodes are connected to each other over the screws of the lens. One half of the central electrode (CE1) needs to be supplied with both the DC (float) voltage, which allows the lens to focus the ion beam, and the HV pulse. This is supplied by a second coaxial cable. The other central electrode (CE2) needs to be supplied by the same DC voltage, but not with the pulse. Therefore, the two halves are connected over a 1 MΩ resistor, allowing the DC voltage to supply both parts but preventing the current from the HV pulse from flowing to the second part. CE1 is supplied directly with the DC voltage, whereas CE2 is supplied with it via the 1 MΩ resistor. Since the resistance to ground is many orders of magnitude higher, very little potential is lost. This setup requires only two coaxial cables to supply four electrodes. In addition, multiple resistors and capacitors were attached to the new lens between the different electrodes and shielding of the coaxial cables to minimise the interferences of the voltage pulse with the adjacent electrodes. This was necessary because the lens with the two outer electrodes and the central electrodes acts as two capacitors in a series. Applying a pulse to CE1 therefore influences the voltages on the outer two electrodes. As the outer electrodes are held on drift potential and are connected to the drift tubes which measure over 1 m, a substantial number of ions would be influenced by the pulse. This could affect the relation between TOF and mass-over-charge ($m/q$) ratio in an uncontrollable way, which would no longer allow for an accurate mass calibration of the spectra. It was therefore crucial to suppress the reaction of the outer electrodes to the pulse, which was realised by connecting CE1 with the outer electrodes through dampening circuits. The connections were doubled, such that each outer electrode is connected over two identical pathways to CE1, each consisting of a capacitor and a resistor in series. In addition, the shielding of the coaxial cable carrying the drift voltage for the outer electrodes was treated similarly and connected to CE1 over a capacitor and resistor as well. Simulations of the current setup predicted drift oscillations with amplitudes of around 4 $V_{PP}$. Two images of the installed lens are shown in Fig. 3. Fig. 3a shows the lens with its surroundings and in Fig. 3b the new lens is shown close up.

The coaxial cable providing the inner electrodes with their floating potential and one half with the HV pulse is connected to the UHV feed-through of the vacuum chamber. Outside of the chamber, the cable is connected to the HV pulser, a fast high-voltage switch built in-house. The pulser box is connected to an Arbitrary Function Generator (AFG31052, Tektronix Inc., USA) which itself is connected to a computer via an Ethernet connection. The setup can be seen in Fig. 4, and it will be explained in the following.

A software featuring a graphical user interface (GUI) was written to make the selection of mass lines and the subsequent process of

selective mass blanking as user-friendly as possible. With the GUI, the user can simply read in previously recorded time-of-flight spectra and click on the mass line or lines that they want to blank. There is no limit to the number of mass lines blanked per spectrum. One only needs to keep in mind that for mass lines which are closer together than the smallest possible pulse width (around 45 ns) it is not possible to blank one without affecting the other. Blanking them together, however, can easily be achieved by using one longer pulse instead of two short ones. If required, the user can adjust the pulse widths and the pulsing times manually. When the peak selection is finished, the software will generate the corresponding waveform, a sequence of zeros and ones. All waveforms have a length of 50 μs, half the length of the spectra recorded by the detector (100 μs) because L3 is situated in the middle of the ion trajectory. Blanking, e.g., a mass line with a TOF of 40 μs in the recorded spectrum will require a pulse to be sent to L3 at 20 μs after the laser shot was fired. A 50 μs waveform contains 16'384 samples, meaning that the behaviour of the waveform can be changed every $\sim 3$ ns. When no pulse is required, the waveform entries are simply set to 0, otherwise to 1. The computer-generated waveform can then be sent to an Arbitrary Function Generator (AFG). When triggered, the AFG will output 0 V and 2.5 $V_{pp}$ for the zeros and ones in the waveform, respectively. The pulse amplitude needs to be further amplified and inverted to $-400$ $V_{pp}$, which is handled by the HV pulser. To support pulses of adjustable length, the HV pulser needs to receive an ON and OFF signal to start and stop providing the pulse voltage, respectively. It is therefore necessary to send two waveforms with the AFG to the HV pulser. The time delay between the ON and OFF pulses provided by the AFG will determine the pulse width of the HV pulse. Supported pulse widths range from 30 ns up to > 25 μs. The AFG is triggered by the same signal from the laser as the acquisition card and will therefore output the waveforms whenever a laser shot is fired. A bias tee adds the pulse HV to the nominal lens DC voltage and provides both to the lens inside the vacuum chamber. By switching off the channels of the AFG, which can be controlled remotely over the laboratory computer, LMS-GT can be used just like before the installation of the pulser and no pulses will be sent to L3. The HV pulser Printed Circuit Board (PCB) is stored in a case to protect it from damage and mounted just outside of the vacuum chamber.

## 3. Performance of mass-selective beam blanking

### 3.1. Pulse characteristics

The characteristics of the blanking pulse provided by the HV switch were analysed with an oscilloscope (Keysight DSOX2002A, 70 MHz, 2 GS/s). The shortest pulses possible to output with the HV pulser have widths of around 45 ns with rise and fall times of 15 ns (measured when the time difference between the ON and OFF trigger pulses sent by the AFG is set to 30 ns, which is the minimally allowed time difference supported by the HV pulser). Longer pulses are supported as well, with tests run up to pulse widths of 20 μs. The rise and fall times increase only slightly for longer pulses, reaching 40 ns for a 20 μs blanking pulse. The HV pulser only provides pulses with voltage amplitudes of $-400$ V. For long pulses, the amplitudes decrease a little, reaching only $-380$ V for a 20 μs blanking pulse. Furthermore, the pulse amplitude experiences a drop with time with a rate of 2.5 V/μs. Both drops in amplitude were accounted for by choosing a slightly higher pulsing amplitude ($-400$ V) than what would suffice to reach 100% blanking efficiency according to simulations run with the ion optical software SIMION. The HV pulser can provide several blanking pulses in a row, with arbitrary pulse widths and without being restricted to fulfil any periodicity, to support blanking several mass lines of one spectrum.
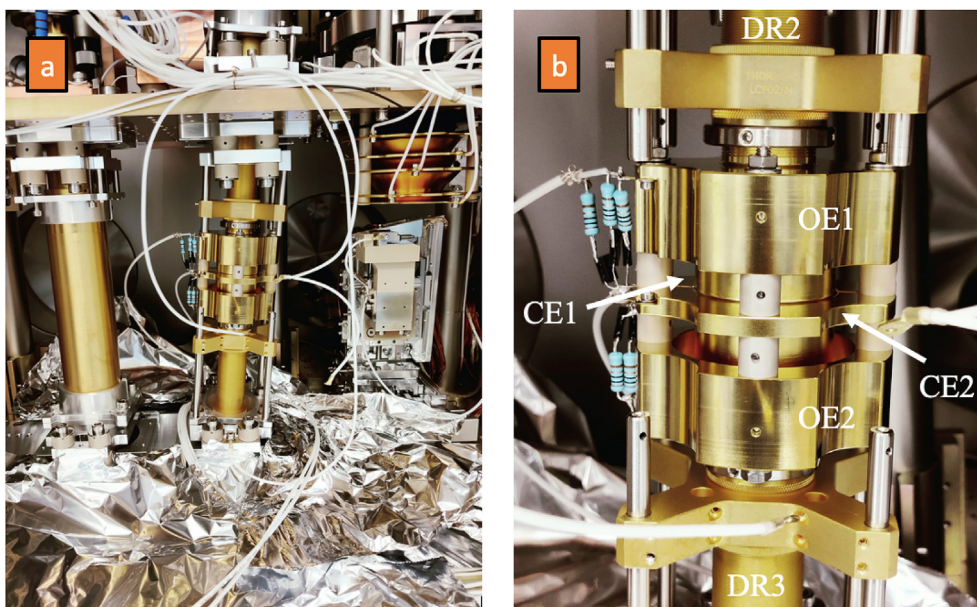
**Fig. 3.** Images of the new lens L3 installed in the vacuum chamber. a) New lens with surroundings. To the right the ion source with the sample stage can be seen. The ions pass from top to bottom through the lens. b) New lens close up with labels in agreement with Fig. 2. The central electrode is divided into two parts. Two coaxial cables supply the lens with the drift and float voltage as well as with the pulse. Several resistors and capacitors were soldered to the different electrodes to minimise interferences from the voltage pulse. The coaxial cables of the new lens are not yet connected to the corresponding power supplies of the instrument.
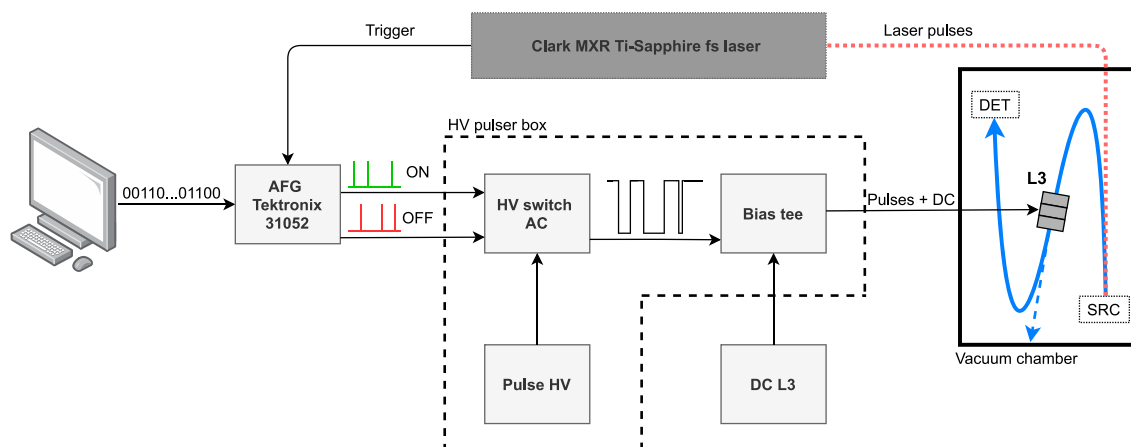


**Fig. 4.** Procedure from the selection of mass lines to blank up to the actual blanking with the lens L3. The information on the mass lines selected for blanking is translated by the computer into waveforms, which will be sent to the Arbitrary Function Generator (AFG). The AFG provides ON and OFF pulses to the HV pulser that will then start and stop providing the blanking pulse, respectively, with amplitudes of − 400 V. A bias tee adds the pulses to the DC voltage of the lens. If the lens receives a pulse the ion beam will experience a deflection and will no longer hit the detector.

### 3.2. Blanking efficiency

To derive the efficiency of the mass-selective blanking device, test measurements were conducted with a NIST SRM661 steel sample, a NIST SRM664 high-carbon steel sample, and a NIST SRM665 high-purity electrolytic iron sample. The SRM certificates of analysis provide certified quantitative information on the elemental composition of the samples, while also providing upper limits for additional elements that could not be certified. A table with the atomic abundances in these three samples is provided in Appendix A in Table 1. In this study, both the certified and estimated abundances were used. The process of sample preparation has been described in a previous study [24]. The most abundant species in the three NIST samples SRM661, SRM664 and SRM665 is iron with weight fractions of 95.6%, 96.7% and 99.9%, respectively (not certified, abundance determined by weight difference). The iron abundances of the three

samples given in atomic fractions are 94.1%, 94.1% and 99.8%, respectively. TOF spectra were recorded with and without blanking certain mass lines and compared to each other to find the blanking efficiency. Relative quantification of non-blanked elements was performed to investigate whether the mass lines adjacent to the blanked one were affected by the voltage pulse.

Fig. 5 shows two examples of blanked mass lines in spectra obtained with the NIST SRM661 sample, with the mass lines selected for blanking being $^{12}$C in Fig. 5a and 56Fe in Fig. 5b. In both figures, the spectrum recorded without blanking the specified mass line is shown in blue, whereas the blanked mass spectrum is shown in red (inverted). The displayed mass range was limited to show a few surrounding peaks. The spectra shown in Fig. 5a were not recorded at the same detector voltage as the spectra in Fig. 5b, which explains the lower peak intensity of $^{56}$Fe compared to $^{12}$C. In both Fig. 5a and b the mass line selected for blanking was removed
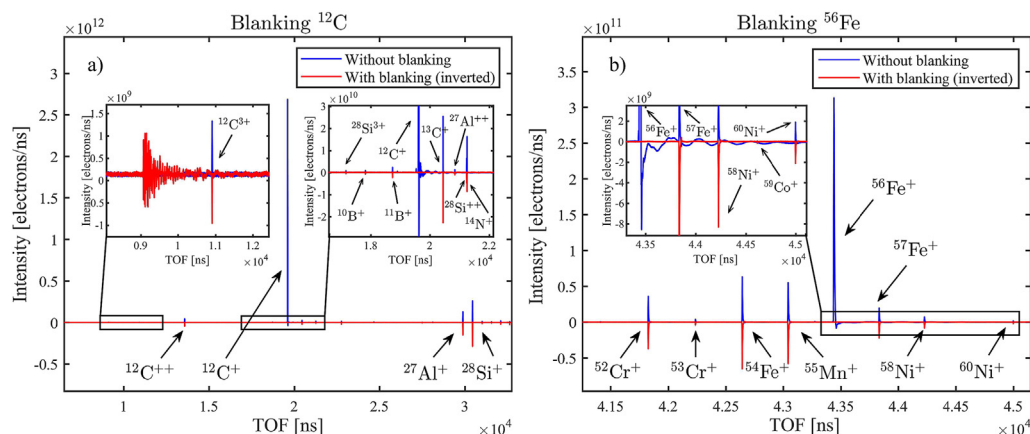
**Fig. 5.** TOF spectra of a NIST SRM661 standard reference material showing the successful blanking of $^{12}C$ (Fig. 5a) and $^{56}Fe$ (Fig. 5b). The blue lines show the TOF spectra recorded without blanking any mass lines whereas the red lines show the (inverted) TOF spectra recorded with blanking $^{12}C$ and $^{56}Fe$, respectively. Inserts show details of the mass spectra on a smaller scale to emphasise the noise introduced by the blanking pulse (upper left panel in Fig. 5a) and the removal of the peaks together with their baseline distortions (upper right panel in Fig. 5a and upper left panel in Fig. 5b).

with 100% efficiency in the blanked spectrum. The areas around the blanked peak are additionally shown on a smaller scale (upper right insert in Fig. 5a and upper left insert in Fig. 5b) to emphasise the removed baseline distortions and oscillations in the blanked spectrum. At the same time, the intensities of the neighbouring peaks were not affected by the pulse. It is possible to blank any mass line on the mass scale, with tests conducted from hydrogen up to lead. The beam blanking device hence fulfils both its objectives. First, to reduce the baseline distortions after a highly intense peak by blanking the corresponding peak. And second, to allow for a safe increase of the detector gain by removing intense peaks. Furthermore, any number of mass lines can be blanked in a spectrum, which allows for an even bigger increase in detector gain compared to when only the most abundant species is blanked. The actual possible increase in detector gain depends on the sample, the number of blanked mass lines and the corresponding abundances.

### 3.3. Noise introduced by the blanking pulses

From a theoretical point of view, it is not possible to produce a perfectly rectangular pulse without over- and undershoots followed by oscillations due to the Gibbs-phenomenon [41]. Pulses usually also introduce ringing on the signal lines if an impedance mismatch is present. The influence of the pulse and its oscillations on adjacent electrodes was investigated. The Einzel lens can be interpreted as two capacitors in a series, and if a pulse is added to the connection in-between theses capacitors, representing the central electrode of L3, the outer lines will react to the change in charge. Therefore, if the pulse is followed by oscillations, also the outer lens electrodes will start to oscillate in a similar manner. Since the outer lens electrodes are held on drift potential, everything else on this potential will start oscillating as well, which is especially problematic for the drift tubes and the detector. Oscillating electric fields will affect the ion trajectories and therefore the time-of-flight recorded by the acquisition system and a shift in TOFs in the blanked spectra with respect to TOFs recorded when no mass lines were blanked are possible. Prior to the installation of the beam blanking device, it was not certain whether precise mass calibration would still be possible when blanking certain mass lines in a spectrum, because the mass-to-time relation might change for certain values of $m/q$. Tests showed, however, that there are no deviations in the time-of-flights between the spectra. Because we minimised the electrical interference from the centre electrodes to the outer

electrodes by suitable electric filtering, the HV pulser does not negatively impact the ion times-of-flight and the TOF spectra can therefore be mass calibrated with the usual accuracy.

Further tests showed that after a pulse of $-400$ V the drift potential (with respect to chamber ground) experienced damped oscillations with initial amplitudes of 8 $V_{pp}$, decreasing to 4 $V_{pp}$ after around 200 ns and stabilising again after around 1.5 µs. Oscillations were also found on the signal line from the detector to the acquisition card with initial amplitudes of 700 $mV_{pp}$. After around 400 ns the oscillations were damped to values below 200 $mV_{pp}$. Since these amplitudes are comparable to the signal strengths of several 100 to 1000 ions hitting the detector, the HV pulser will introduce noise to the recorded TOF spectra. The introduced noise can be seen in Fig. 5a, where the time window around $0.8-1.2$ µs is scaled up and shown in the upper left insert. The noise occurs when the mass line is blanked, approximately at half the recorded TOF of the blanked $^{12}C$. The noise does not influence the adjacent mass line, which belongs to triply charged $^{12}C$, but it could possibly obscure some smaller mass lines occurring at the same time. However, it seems possible to cope with the loss of one single, low intensity mass line, seeing that the selective mass blanking device should allow for a safe increase of the detector gain. This has the potential to uncover other mass lines at any other point in the spectrum previously hidden in the background.

The spectra shown in Fig. 5a were background corrected by recording and subtracting of a blank spectrum. The noise introduced by the mass-selective blanking device was reduced to a large part by this procedure, as visualised in Fig. 6. The blue line shows part of a mass spectrum obtained with the NIST SRM661 before background subtraction and the red line shows the same part of the spectrum after the subtraction of a blank spectrum. For reference, the signal intensity of the $^{56}Fe$ mass line (not shown) is at a level of $1.5 \cdot 10^{12}$ electrons/ns. No specific mass line was blanked in this spectrum; it was recorded to study the noise reduction by background subtraction. With the background subtraction, one can reduce the noise intensity by a factor 100 to the level of around $10^9$ electrons/ns. The background subtracted spectrum around 2.125 µs is shown enlarged in the lower right corner of the figure. It shows that by subtracting the background two peaks were recovered, corresponding to doubly charged $^{28}Si$ and singly charged $^{14}N$. Since the baseline is at the level of $10^7$ electrons/ns peaks with intensities up to $10^9$ electrons/ns can still be hidden by the pulser noise. However, the noise introduced by the pulser is manageable and is a good trade-off for an improved LoD of the instrument.
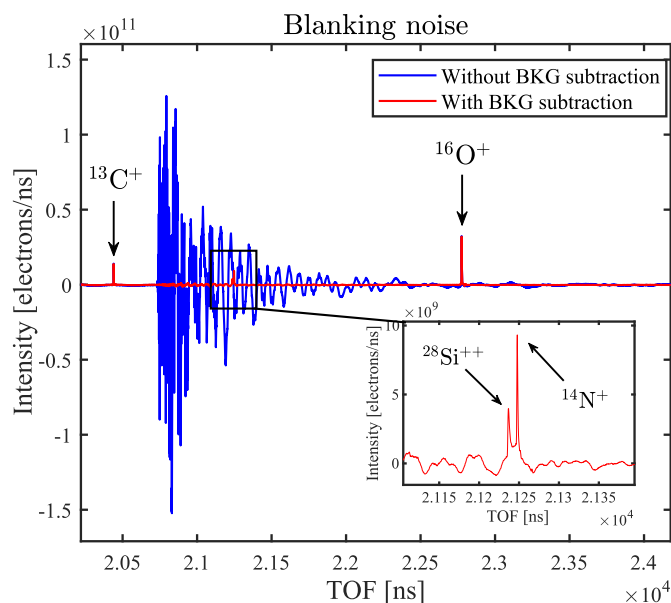
**Fig. 6.** Noise introduced by the blanking pulser and measured by the acquisition system. The blue line shows the spectrum as recorded whereas the red line shows the spectrum to which a background subtraction was applied. The background subtracted spectrum around 2.125 μs is shown on a different scale in the lower right corner to point out the recovered mass lines of doubly charged $^{28}$Si and singly charged $^{14}$N.

If the electronic noise does interfere with a mass of interest, there are ways to retrieve the information at that specific TOF. For example, one could for example start the blanking pulse a bit earlier such that the noise occurs at an earlier TOF which does not interfere with the mass of interest. The blanking pulse simply needs to be chosen a bit longer to still be able to blank the intense mass peak. The noise arises only due to the change in the potentials, once the voltages are stable again the noise is not significant anymore, a longer blanking pulse does therefore not prolong the blanking noise. After acquiring a spectrum with this method, it can then be combined with the initial spectrum where the mass of interest was hidden, yielding a spectrum free of blanking noise.

### 3.4. Relative sensitivity coefficients (RSCs) and quantitative measurements

The ion yield of the laser ablation ionisation process is element dependent, as is the detection sensitivity. For quantitative atomic concentration determination, the calculation of relative sensitivity coefficients (RSCs), defined as the ratio between measured and reference abundance, is required. Previous studies of the LMS-GT instrument have shown that it is able to perform quantitative measurements with RSCs using reference samples with [24,38]. It was investigated whether the previously determined general performance of LMS-GT was compromised by the introduction of the modified Einzel lens and the HV pulser electronics. An RSC campaign was conducted on the NIST steel sample SRM664 (atomic iron fraction of 94.1%), and data were acquired with and without blanking the $^{56}$Fe mass line. The laser output power was set to 30 μJ and the detector voltage to 2100 V. 10 craters were ablated with and without blanking and per crater 40'000 laser shots were applied. For the analysis, 20'000 shots were averaged per crater. The first 1'000 applied shots were not considered in the analysis to account for surface contaminations and crater formation processes. The resulting RSCs with respect to the standard elemental abundance

and the calculated elemental abundance are shown in Fig. 7. Out of the detected elements, only the ones certified by NIST are shown.

As Fig. 7 shows, the calculated RSCs are very similar for both the measurements with and without blanking the $^{56}$Fe mass line. No blanking mode gives better RSC values, i.e., RSCs closer to 1. Measurements with two other NIST standard reference samples (SRM661 and SRM665), which contain more trace elements, showed equivalent results for high abundance species but experienced a bigger scatter between the blanked and non-blanked measurements for low abundant species. This can be attributed to the inhomogeneity of the sample at micrometre scales for elements at the lower ppm level and below. At these scales, it is no longer possible to isolate the influence of the inhomogeneity on the RSC calculation from a possible influence of the mass selective blanking device. Reliable conclusions about the influence of the blanking device on the RSC calculations can therefore only be drawn at scales which are not affected by the inhomogeneity. To get the same reliability for trace elements a larger sample area would need to be studied.

RSC scores were calculated for both measurements shown in Fig. 7 according to the following formula:

$$RSC\ score = \left(1 - \left(\frac{1}{N}\sum_{i=1}^{N}\frac{|1 - RSC_i|}{1 + RSC_i}\right)\right) \cdot 100\ \%$$

with $N$ being the number of elements considered, allowing for a comparison between different sets of RSC values. The resulting RSC scores with and without blanking the $^{56}$Fe mass line are $(59.75 \pm 0.36)\%$ and $(58.22 \pm 0.49)\%$, respectively.

The dependence of the RSCs on the detector voltage was previously investigated and no trend was found [24]. The measurements were repeated with blanking the $^{56}$Fe mass line to ensure that the detector voltage would not impact the performance of mass-selective blanking. Being able to use the mass-selective blanking device
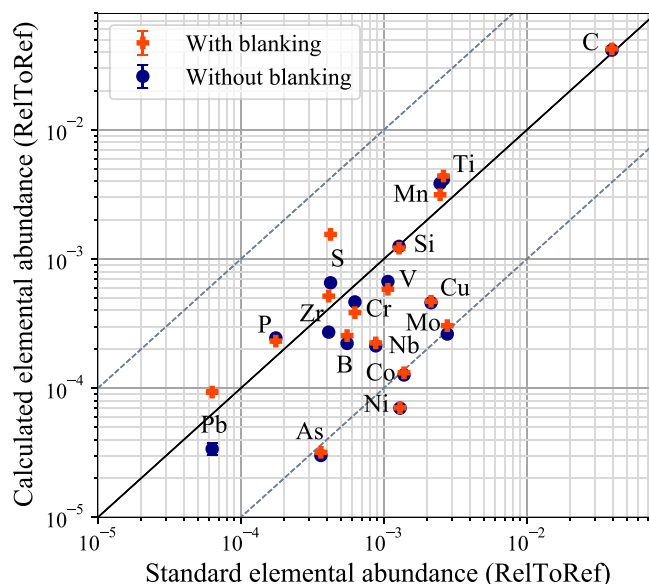


**Fig. 7.** RSC comparison for measurements conducted on a NIST SRM664 steel sample with (red crosses) and without (blue circles) blanking the $^{56}$Fe mass line. The laser output power was set to 30 μJ and the detector voltage to 2100 V. Ten craters were analysed for each blanking mode (with blanking and without blanking) and 20'000 spectra were averaged per crater, with the first 1'000 shots applied on the sample not considered. The solid diagonal line represents perfect RSC values of 1, where the calculated abundance equals the standard abundance. The dashed diagonal lines mark calculated abundance deviations of a factor 10 from the standard abundance, which is equivalent to RSC values of 10 (upper dashed line) and 0.1 (lower dashed line). Only certified elements are shown.

independent of the detector voltage is important for future measurement campaigns, since it means voltage campaigns to find the optimal parameters for blanking prior to the measurements are not required. This is especially important as the mass selective blanking device will allow for an increase in detector voltage and comparisons to non-blanked measurements are only possible if the detector voltage does not influence the blanking process. Six detector voltages in-between 1900 V and 2150 V, in steps of 50 V, were chosen and the calculated abundances of selected species were compared to the standard abundances. The applied laser pulse energy was 1 μJ after transmission losses. The results are shown in Fig. 8. In Fig. 8a, the data with $^{56}$Fe mass line blanking are shown, whereas on Fig. 8b data no blanking was used. The results obtained with blanking do not vary significantly from the results where no blanking was applied. In Fig. 8a, the values are slightly more scattered for certain elements as, e.g., Co, Cu, and Mo, however, this could be an artefact of the small statistics as only 3 craters were studied per blanking mode and the size of the sample spots of ∼ 2 μm ⌀ is lower than the expected scale of chemical homogeneity of the sample. The RSCs of these three elements are slightly worse with blanking compared to without blanking, but not for all detector voltages. RSCs of other elements such as P, Mn and Si are slightly better with blanking than without blanking, but again only for certain detector voltages. No general trend can be observed. RSC differences of a factor ∼ 2 can be considered negligible for such small statistics. RSC scores were calculated for both measurements and are summarised in Table 2 in the Appendix. Both measurements show no improvement with any applied detector voltage and the RSC scores of the two blanking modes agree well at each applied voltage.

To conclude, beam blanking does not significantly influence the RSC calculations and the performance of LMS-GT was not compromised by the installation of the mass-selective blanking device. Measurements conducted at different detector voltages show that the blanking process is not influenced by this parameter. The final step is to investigate the new LOD. This will be addressed in the following section.

## 4. Limit of detection with beam blanking

The LoD of the LMS-GT instrument prior to the installation of the mass-selective blanking device was at the ppm level [24]. In few cases, a small number of species with very high ionisation efficiencies were detected at the ppb level. After the installation, a measurement campaign was conducted with a NIST SRM665 sample to investigate the influence of the mass-selective blanking device on the LoD of the instrument. The NIST SRM665 was chosen since it has a large number of trace elements with atomic abundances below 1 ppm. The laser output power was set to 6 μJ. Spectra were recorded with and without using the newly installed beam blanking device. When no mass lines were blanked, the detector voltage could maximally be set to 2100 V without risking detector damage due to saturation. In blanking mode, the detector voltage was set to 2300 V and the mass lines $^{54}$Fe, $^{56}$Fe and $^{57}$Fe were blanked. NIST SRM665 has an iron abundance of 99.9 wt% (atomic fraction of 99.8%, not certified, determined by weight difference), therefore, blanking the most abundant iron isotopes allows to increase the detector voltage which yields a higher detector gain and should lead to an improved LoD. In the following analysis, only elements with abundances below 1 ppm were considered. In each blanking mode (with and without blanking the iron mass lines) 50 craters were studied on the sample, with the distance between the craters set to 50 μm. Fig. 9 visualises in how many out of the 50 craters the analysed elements were found, with the elements sorted in descending order of their atomic abundance (indicated below the figure). It has to be kept in mind that the given element abundances were not certified by NIST because they were either not detected or, as in the case of Nb, only detected with one analytical method, which does not suffice for certification. The given abundances must therefore be seen as upper limits, and the actual element abundances in the NIST SRM665 sample might he much lower than what is stated below Fig. 9. Nevertheless, comparing the two measurements, a clear improvement can be seen when blanking is applied. These first results demonstrate that the LoD improved by using the mass-selective blanking device, showing detections down to the single ppb range. The data were analysed using a thoroughly tested MATLAB analysis software for time-of-flight mass spectrometry written in-house [42].

Measurements of elements in the lower ppb range are challenging because of chemical inhomogeneities of the sample on the spatial scale probed by the laser and the limited ablated mass per laser shot. While the NIST materials were produced to achieve the highest level of homogeneity, compositional heterogeneities are present within all
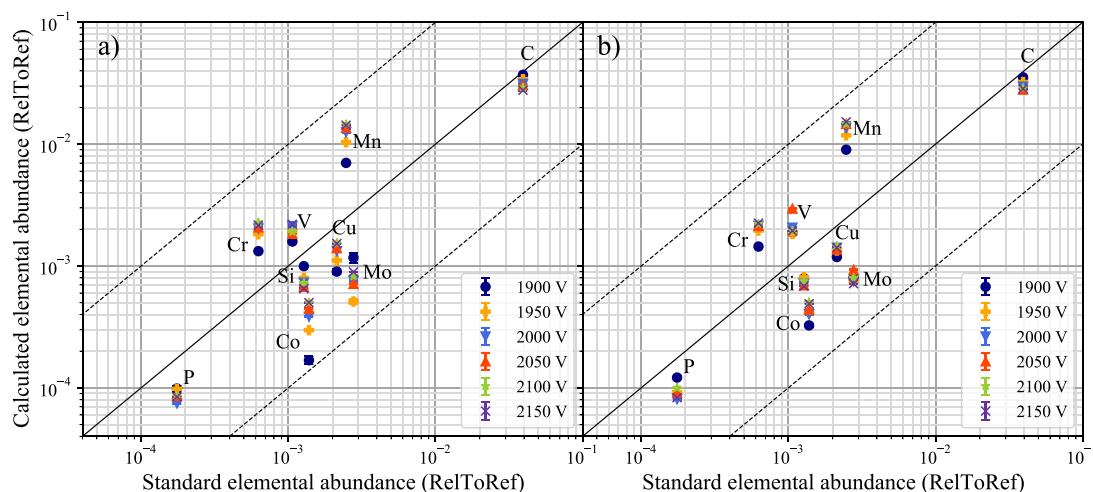


**Fig. 8.** Calculated and standard elemental abundances relative to a reference species of selected species measured with six different detector voltages on a NIST SRM664 sample. Each data point represents the average of 3 × 20′000 shots. The solid diagonal line represents perfect RSC values of 1, where the calculated abundance equals the standard abundance. The dashed diagonal lines mark calculated abundance deviations of a factor 10 from the standard abundance, which is equivalent to RSC values of 10 (upper dashed line) and 0.1 (lower dashed line). a) The $^{56}$Fe mass line was blanked. b) No mass line was blanked; these results were reproduced from Ref. [24].
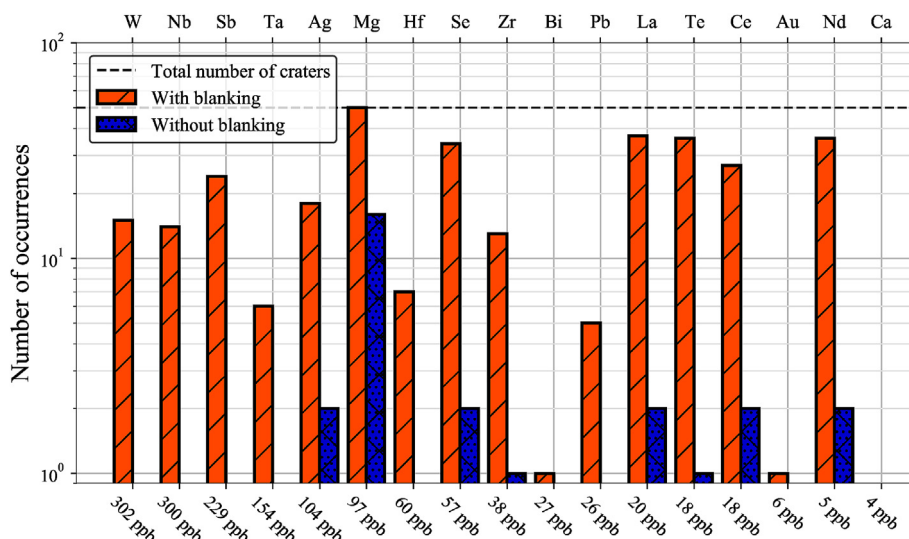
**Fig. 9.** Element detection on the NIST SRM665 sample with and without blanking the $^{54}$Fe, $^{56}$Fe and $^{57}$Fe mass lines. Applied laser output power after transmission losses was 6 μJ. The applied detector voltage was 2300 V in blanking mode and 2100 V while not blanking. Each bar represents the data obtained from 50 craters which were ablated with a burst of 4800 single laser shots each (240′000 laser shots per bar). Abundances are given in atomic fractions, sorted in descending order. The number of occurrences on the y-axis are visualised on a logarithmic scale.

three studied samples. Perfect homogeneity at the micrometre scale cannot be guaranteed and the measurements presented here are sensitive to this inhomogeneity [43,44]. From an interferometry and scanning electron microscopy (SEM) analysis of the craters, the mean ablated mass per laser shot with an applied laser output power of 6 μJ was determined to be ∼ 10 fg. For a low abundant element in the NIST SRM665 sample, such as Au with an atomic fraction of 6 ppb, this implies that, statistically speaking and assuming total homogeneity of the sample, out of all the atoms ablated in one laser shot only 1 atom belongs to gold. This is of course only a theoretical estimation, as the sample is not homogeneous down to atomic levels. The bigger the inhomogeneity, the harder it becomes to accurately determine RSCs of low abundant species. It is therefore necessary to analyse a large enough sample volume to obtain the required statistics. The detection of low abundant elements is further complicated by the limited ionisation rate of the instrument. In addition, not all elements ionise equally well, which can make detections of species with a lower ionisation efficiency more challenging and leads to element dependent LoDs. To determine the quantitative improvement of the instrument's LoD by the installation of the beam blanking device more data must be collected in the future. The detection of trace elements and their isotopes at these concentration levels open a variety of new applications for LIMS, including material dating, detailed analysis of the formation processes of rocks and studies of grain sized material such as microfossils, e.g. in the Gunflint chert previously studied with LMS [45,46]. Furthermore, high sensitivity depth profiling is possible [22,47]. Switching from infrared to UV laser pulses should increase the ionisation rate and therefore the detection capabilities of the instrument and improve the RSC calculations [20]. The ionisation rate could be further improved by a double pulse (DP) laser system as it has been shown for the LMS instrument [21−23]. These first results show the improvement of LMS-GT's detection limit and emphasise its potential to detect species in the single digit ppb (atomic fractions) range.

## 5. Conclusion

This study reported the successful installation of a mass-selective blanking device in the LMS-GT instrument, a femtosecond laser ablation and ionisation mass spectrometer (fs-LIMS).

With a blanking device, single mass lines in a mass spectrum can be removed from the spectrum with a fast voltage switch, which deflects the ion beam for a short amount of time such that the corresponding ions do not reach the detector. The mass lines can conveniently be selected for blanking through the GUI of in-house written software with which a previously recorded spectrum can be read in, and with a mouse-click on a mass line it gets selected for full suppression. The program translates the information on the selected mass lines into waveforms and sends them over an Arbitrary Function Generator (AFG) to a HV pulser designed in-house. The HV pulser applies blanking pulses to a modified Einzel lens located in the middle of the ion trajectory at a time focus. Ions flying through the lens while the HV switch is pulsing the lens experience a different electric field that alters their trajectory such that they no longer reach the detector. By timing the fast voltage pulses with the time-of-flight of the ions, single mass lines can be blanked. Several peaks can be simultaneously removed from one spectrum. The adjacent mass lines remain unaffected by the blanking pulse. Blanking the most abundant peaks in a spectrum allows to safely increase the detector gain to a certain extent, limited by the intensities of the remaining peaks.

The installation of the blanking device did not compromise the current performance of LMS-GT, i.e., it did not introduce major noise or influence the times-of-flight of the ions, nor did it negatively affect the capabilities of RSC calculations. It did, however, make it possible to improve the LoD of LMS-GT , pushing it to the lower ppb range, by allowing to safely increase the detector gain while blanking the most abundant mass peaks. Selective beam blanking can be achieved with 100% efficiency over a mass range from 1 to ∼ 250 amu, equivalent to a maximum suppression by four to five orders of magnitude to below the noise floor. At analytical spot sizes of ∼ 2 − 10 μm the performance of LMS-GT starts to compete with the ones of TOF-SIMS and dynamic SIMS [11].

Further studies are required to determine the improvement quantitatively. The number of reported detections in the single digit ppb range emphasise the big potential of the LMS-GT instrument and the LIMS technique in general. The detailed analysis of trace elements in micrometre inclusions is of high interest in many academic and industrial fields, including the semiconductor industry and geology. Geological samples, including those from celestial bodies, are key

elements to determine the age and formational processes of our Solar System as well as the origin of life on Earth. Especially for dating, the accurate determination of trace elements (isotopes) is crucial. Although so far only metallic samples have been tested, the mass-selective blanking device is expected to work equally well for any other solid sample. For geological samples, where usually not a single, high-intensity peak is present but many peaks with similar intensities, the best way to use the blanking device would be to either blank several peaks simultaneously or several mass peaks in a row, i.e., remove the peaks of a complete mass range up to a certain mass. This would allow for the study of heavy trace elements at an increased detector gain. With the extension of the blanking device, LMS-GT has become a powerful instrument to study trace elements on the micron scale in any solid sample.

## Author statement

**Salome Gruchola:** Conceptualization, Methodology, Software, Investigation, Writing − original draft.

**Coenraad P. de Koning:** Software, Validation, Investigation, Resources, Writing − review and editing.

**Reto Wiesendanger:** Conceptualization, Methodology.

**Peter Keresztes Schmidt:** Software, Writing − review and editing.

**Andreas Riedo:** Resources, Writing − review and editing.

**Valentine Grimaudo:** Resources, Writing − review and editing.

**Rustam A. Lukmanov:** Writing − review and editing.

**Niels F.W. Ligterink:** Writing − review and editing.

**Marek Tulej:** Validation, Writing − review and editing, Supervision.

**Peter Wurz:** Conceptualization, Validation, Resources, Writing − review and editing, Supervision, Project administration, Funding acquisition.

## Declaration of competing interest

The authors declare that they have no known competing financial interests or personal relationships that could have appeared to influence the work reported in this paper.

## Acknowledgment

## Appendix

**Table 1**

Elemental abundances in the three NIST standard reference materials 661, 664 and 665. The values of the atomic abundances are given in ppm. The certified element abundances are shown in italics.

| Element Name | Element Mass | NIST SRM661 | NIST SRM664 | NIST SRM665 |
| --- | --- | --- | --- | --- |
| H | 1.00794 | 272.69 | *269.47* | *276.74* |
| B | 10.811 | 26.24 | *552.73* | 6.71 |
| C | 12 | *17957.10* | 39384.06 | 371.92 |
| N | 14.0067 | 145.21 | 116.35 | 79.66 |
| O | 15.9994 | 30.92 | 57.72 | 244.08 |
| Mg | 24.305 | 2.26 | 2.24 | 0.46 |
| Al | 26.9815386 | *427.84* | 161.07 | *14.47* |
| Si | 28.0855 | *4364.70* | 1276.57 | *158.91* |
| P | 30.973762 | *266.21* | 175.38 | *36.02* |
| S | 32.065 | 257.15 | 423.54 | 102.65 |
| Ca | 40.078 | 1.37 | 1.36 | 0.14 |
| Ti | 47.867 | 229.68 | *2610.20* | 6.99 |
| V | 50.9415 | *118.70* | *1066.38* | 6.57 |
| Cr | 51.9961 | 7294.74 | 626.85 | *75.10* |
| Mn | 54.938045 | 6603.93 | 2472.00 | 57.88 |
| Fe | 55.845 | 941033.39 | 940642.53 | 997979.46 |
| Ni | 58.6934 | 18637.83 | 1295.75 | 389.70 |
| Co | 58.933195 | *298.48* | 1382.65 | 66.26 |
| Cu | 63.546 | *363.32* | 2137.15 | *50.92* |
| Zn | 65.409 | 0.84 | 8.31 | 2.56 |
| Ge | 72.64 | 45.41 | 22.44 | 38.40 |
| As | 74.9216 | *124.73* | *362.53* | *1.49* |
| Se | 78.96 | 27.85 | 2.06 | 0.07 |
| Zr | 91.224 | *54.23* | *410.89* | 0.06 |
| Nb | 92.90638 | *130.17* | *877.06* | 0.30 |
| Mo | 95.94 | *1088.64* | *2774.46* | *29.07* |
| Ag | 107.8682 | *2.04* | 0.10 | 0.10 |
| Sn | 118.71 | 50.94 | 22.88 | 2.35 |
| Sb | 121.76 | 18.96 | 156.15 | 0.23 |
| Te | 127.6 | *2.58* | 0.85 | 0.04 |
| La | 138.90547 | *1.58* | *0.27* | 0.02 |
| Ce | 140.116 | *5.10* | 0.97 | 0.02 |
| Pr | 140.90765 | 0.55 | 0.12 | 0.02 |
| Nd | 144.242 | *1.14* | 0.45 | 0.02 |
| Hf | 178.49 | 0.62 | 15.22 | 0.06 |
| Ta | 180.94788 | *60.76* | *330.23* | 0.15 |
| W | 183.84 | 50.83 | *295.49* | 0.30 |
| Au | 196.966569 | 0.14 | *0.28* | 0.01 |
| Pb | 207.2 | *0.07* | 62.92 | *0.03* |
| Bi | 208.9804 | *1.05* | 2.34 | 0.03 |

**Table 2**

RSC scores for different applied detector voltages, compared between measurements conducted with blanking the $^{56}$Fe mass line and without blanking it. The applied laser pulse energy was 1 μJ after transmission losses. Errors were determined by error propagation.

| Applied voltage | RSC score with blanking $^{56}$Fe | RSC score without blanking |
|---|---|---|
| 1900 V | $(65.99 \pm 1.10)$ % | $(64.75 \pm 0.68)$ % |
| 1950 V | $(59.68 \pm 0.37)$ % | $(62.25 \pm 0.35)$ % |
| 2000 V | $(58.96 \pm 0.27)$ % | $(59.16 \pm 0.24)$ % |
| 2050 V | $(60.16 \pm 0.18)$ % | $(58.45 \pm 0.16)$ % |
| 2100 V | $(61.10 \pm 0.14)$ % | $(61.56 \pm 0.14)$ % |
| 2150 V | $(60.04 \pm 0.14)$ % | $(59.26 \pm 0.11)$ % |

# References

[1] P. Chakraborty, T. Pradeep, The emerging interface of mass spectrometry with materials, NPG Asia Mater. 11 (1) (2019) 48, https://doi.org/10.1038/s41427-019-0149-3.

[2] C.A. Heinrich, et al., Quantitative multi-element analysis of minerals, fluid and melt inclusions by laser-ablation inductively-coupled-plasma mass-spectrometry, Geochem. Cosmochim. Acta (2003), https://doi.org/10.1016/S0016-7037(03)00084-X [Preprint].

[3] P.T. Palmer, T.F. Limero, Mass spectrometry in the U.S. space program: past, present, and future," in, J. Am. Soc. Mass Spectrom. (2001), https://doi.org/10.1016/S1044-0305(01)00249-5.

[4] P. Wurz, et al., Mass Spectrometric Analysis in Planetary Science: Investigation of the Surface and the Atmosphere, " Solar System Research, 2012, https://doi.org/10.1134/S003809461206007X [Preprint].

[5] R. Arevalo, Z. Ni, R.M. Danell, Mass spectrometry and planetary exploration: a brief review and future projection, J. Mass Spectrom. (2020) https://doi.org/10.1002/jms.4454 [Preprint].

[6] N.F.W. Ligterink, et al., ORIGIN: a novel and compact Laser Desorption − mass Spectrometry system for sensitive in situ detection of amino acids on extraterrestrial surfaces, Sci. Rep. 10 (1) (2020) 1−10, https://doi.org/10.1038/s41598-020-66240-1.

[7] A. Riedo, et al., The Detection of Elemental Signatures of Microbes in Martian Mudstone Analogs Using High Spatial Resolution Laser Ablation Ionization Mass Spectrometry, Astrobiology, 2020, https://doi.org/10.1089/ast.2019.2087 [Preprint].

[8] H. Zhong, et al., Mass spectrometric monitoring of interfacial photoelectron transfer and imaging of active crystalline facets of semiconductors, Nat. Commun. (2017) https://doi.org/10.1038/ncomms14524 [Preprint].

[9] J.N.M.J.C. Miller, Statistics and Chemometrics for Analytical Chemistry Sixth Edition, Clinical Medicine, Journal of the Royal College of Physicians of London, 2009.

[10] P.L. Urban, Clarifying Misconceptions about Mass and Concentration Sensitivity, " Journal of Chemical Education [Preprint, 2016, https://doi.org/10.1021/acs.jchemed.5b00986.

[11] T. Wirtz, et al., High-resolution high-sensitivity elemental imaging by secondary ion mass spectrometry: from traditional 2D and 3D imaging to correlative microscopy, Nanotechnology (2015), https://doi.org/10.1088/0957-4484/26/43/434001 [Preprint].

[12] D. Günther, B. Hattendorf, Solid sample analysis using laser ablation inductively coupled plasma mass spectrometry, TrAC - Trends in Analytical Chemistry [Preprint] (2005), https://doi.org/10.1016/j.trac.2004.11.017.

[13] M. Tulej, et al., On Applicability of a Miniaturised Laser Ablation Time of Flight Mass Spectrometer for Trace Elements Measurements, International Journal of Spectroscopy, 2012, pp. 1−14, https://doi.org/10.1155/2012/234949, 2012.

[14] A.A. Ganeev, et al., Analytical Glow Discharge Mass Spectrometry, " Russian Chemical Bulletin [Preprint, 2012, https://doi.org/10.1007/s11172-012-0107-5.

[15] C.D. Quarles, J. Castro, R.K. Marcus, Glow discharge mass spectrometry," in, Encycl. Anal. Spectrosc. Spectrom. (2016), https://doi.org/10.1016/B978-0-12-803224-4.00056-X.

[16] J. Busam, et al., Application of 7N in as secondary cathode for the direct current-glow discharge mass spectrometry analysis of solid, fused high-purity quartz, J. Mass Spectrom. (2021) https://doi.org/10.1002/jms.4771 [Preprint].

[17] J. Pisonero, B. Fernández, D. Günther, Critical revision of GD-MS, LA-ICP-MS and SIMS as inorganic mass spectrometric techniques for direct solid analysis, J. Anal. Atomic Spectrom. 24 (9) (2009) 1145−1160, https://doi.org/10.1039/B904698D.

[18] Y. Lin, et al., Progress of laser ionization mass spectrometry for elemental analysis — a review of the past decade, Spectrochim. Acta B Atom Spectrosc. 65 (11) (2010) 871−883, https://doi.org/10.1016/J.SAB.2010.08.007.

[19] V.A. Azov, L. Mueller, A.A. Makarov, Laser ionization mass spectrometry at 55: Quo Vadis? Mass Spectromet. Rev. (2020) https://doi.org/10.1002/MAS.21669 [Preprint].

[20] M. Tulej, et al., Current Progress in Femtosecond Laser Ablation/ionisation Time-Of-Flight Mass Spectrometry, Applied Sciences, Switzerland, 2021, https://doi.org/10.3390/app11062562 [Preprint].

[21] M. Tulej, et al., Mass spectrometric analysis of the Mg plasma produced by double-pulse femtosecond laser irradiation, J. Anal. Atomic Spectrom. (2018), https://doi.org/10.1039/c8ja00036k [Preprint].

[22] V. Grimaudo, et al., UV post-ionization laser ablation ionization mass spectrometry for improved nm-depth profiling resolution on Cr/Ni reference standard, Rapid Commun. Mass Spectrom. (2020), https://doi.org/10.1002/rcm.8803 [Preprint].

[23] A. Riedo, et al., Improved plasma stoichiometry recorded by laser ablation ionization mass spectrometry using a double-pulse femtosecond laser ablation ion source, Rapid Commun. Mass Spectrom. (2021), https://doi.org/10.1002/rcm.9094 [Preprint].

[24] C.P. de Koning, et al., Quantitative elemental analysis with the LMS-GT; a next-generation LIMS-TOF instrument, Int. J. Mass Spectrom. (2021) 116662, https://doi.org/10.1016/j.ijms.2021.116662.

[25] J. Nuñez, et al., NanoSIMS for Biological Applications: Current Practices and Analyses, " Biointerphases [Preprint, 2018, https://doi.org/10.1116/1.4993628.

[26] Z. Liang, et al., Tip-enhanced Ablation and Ionization Mass Spectrometry for Nanoscale Chemical Analysis, " Science Advances [Preprint, 2017, https://doi.org/10.1126/sciadv.aaq1059.

[27] M. Hohl, et al., Mass selective blanking in a compact multiple reflection time-of-flight mass spectrometer, Int. J. Mass Spectrom. 188 (3) (1999) 189−197, https://doi.org/10.1016/S1387-3806(99)00040-8.

[28] M. Vestal, et al., A new delayed extraction MALDI-TOF MS-MS for characterization of protein digests, Mass Spectromet. Biol. Med. (2000) 1−16, https://doi.org/10.1007/978-1-59259-719-2_1.

[29] F. Liu, et al., TOF mass spectra of zircon M257 measured by VUV laser desorption ionization, J. Anal. Atomic Spectrom. (2021), https://doi.org/10.1039/D1JA00191D [Preprint].

[30] R. Wiesendanger, et al., Improved detection sensitivity for heavy trace elements using a miniature laser ablation ionisation mass spectrometer, J. Anal. Atomic Spectrom. 32 (11) (2017) 2182−2188, https://doi.org/10.1039/C7JA00193B.

[31] U. Rohner, J.A. Whitby, P. Wurz, A miniature laser ablation time-of-flight mass spectrometer for in situ planetary exploration, Meas. Sci. Technol. 14 (12) (2003) 2159−2164, https://doi.org/10.1088/0957-0233/14/12/017.

[32] T.J. Cornish, R.J. Cotter, Tandem time-of-flight mass spectrometer, Anal. Chem. 65 (1993) 1043−1047. Available at: https://pubs.acs.org/sharingguidelines. (Accessed 30 November 2021).

[33] M.M. Cordero, T.J. Cornish, R.J. Cotter, Matrix-assisted laser desorption/ionization tandem reflectron time-of-flight mass spectrometry of fullerenes, J. Am. Soc. Mass Spectrom. 7 (6) (1996) 590−597, https://doi.org/10.1016/1044-0305(96)00058-X.

[34] R.J. Cotter, et al., Tandem time-of-flight (TOF/TOF) mass spectrometry and proteomics, J. Mass Spectrom. Soc. Jpn. 53 (1) (2005) 7. Available at:/pmc/articles/PMC2922030/. (Accessed 7 December 2021).

[35] S.A. Getty, et al., A compact tandem two-step laser time-of-flight mass spectrometer for in situ analysis of non-volatile organics on planetary surfaces, IEEE Aero. Conf. Proc. (2014), https://doi.org/10.1109/AERO.2014.6836334 [Preprint].

[36] X. Li, et al., Tandem mass spectrometry on a miniaturized laser desorption time-of-flight mass spectrometer, IEEE Aero. Conf. Proc. (2016), https://doi.org/10.1109/AERO.2016.7500615. 2016-June.

[37] A. Riedo, et al., Performance evaluation of a miniature laser ablation time-of-flight mass spectrometer designed for in situ investigations in planetary space research, J. Mass Spectrom. (2013), https://doi.org/10.1002/jms.3104 [Preprint].

[38] R. Wiesendanger, et al., The LMS-GT instrument − a new perspective for quantification with the LIMS-TOF measurement technique, J. Anal. Atomic Spectrom. 34 (10) (2019) 2061−2073, https://doi.org/10.1039/C9JA00235A.

[39] A.W. Szumlas, D.A. Rogers, G.M. Hieftje, Design and construction of a mechanically simple, interdigitated-wire ion gate, Rev. Sci. Instrum. 76 (8) (2005), https://doi.org/10.1063/1.2006308, 086108.

[40] C. Chen, et al., Field switching combined with Bradbury−Nielsen gate for ion mobility spectrometry, Anal. Chem. 87 (2015) 14, https://doi.org/10.1021/acs.analchem.5b01737.

[41] E. Hewitt, R.E. Hewitt, The Gibbs-Wilbraham Phenomenon: an Episode in Fourier Analysis, Archive for History of Exact Sciences, 1979, https://doi.org/10.1007/BF00330404 [Preprint].

[42] S. Meyer, et al., Fully automatic and precise data analysis developed for time-of-flight mass spectrometry, J. Mass Spectrom. 52 (9) (2017) 580−590, https://doi.org/10.1002/JMS.3964.

[43] Heinrich Marinenko, Ruegg, Standard Reference Materials : micro-homogeneity studies of NBS standard reference materials, NBS research materials, and other related samples, 1979, https://doi.org/10.6028/NBS.SP.260-65.

[44] Seward, Mavrodineanu, Standard Reference Materials : Summary of the Clinical Laboratory Standards Issued by the, National Bureau of Standards,

1981, https://doi.org/10.6028/NBS.SP.260-71.

[45] R.A. Lukmanov, A. Riedo, et al., On topological analysis of fs-LIMS data. Implications for in situ planetary mass spectrometry, Front. Artif. Intell. 4 (2021) 119, https://doi.org/10.3389/FRAI.2021.668163/BIBTEX.

[46] R.A. Lukmanov, M. Tulej, et al., Chemical identification of microfossils from the 1.88-Ga Gunflint chert: towards empirical biosignatures using laser ablation ionization mass spectrometer, J. Chemometr. 35 (10) (2021) e3370, https://doi.org/10.1002/CEM.3370.

[47] V. Grimaudo, et al., Depth profiling and cross-sectional laser ablation ionization mass spectrometry studies of through-silicon-vias, Anal. Chem. (2018), https://doi.org/10.1021/acs.analchem.7b05313 [Preprint].